Received: 19 February 2022 | Revised: 14 May 2022 | Accepted: 18 May 2022

DOI: 10.1002/er.8195

RESEARCH ARTICLE

INTERNATIONAL JOURNAL OF ENERGY RESEARCH WILEY

Potential of wood as thermal energy storage materials: Different characteristics depending on the hierarchical structure and components

Jihee Nam | **Beom Yeol Yun** | **Ji Yong Choi** | **Sumin Kim**

Department of Architecture and Architectural Engineering, Yonsei University, Seoul, Republic of Korea

Correspondence
Sumin Kim, Department of Architecture and Architectural Engineering, Yonsei University, Seoul 03722, Republic of Korea.
Email: kimsumin@yonsei.ac.kr

Funding information
Korea Institute of Energy Technology Evaluation and Planning (KETEP), Grant/Award Number: 20202020800030

Summary

Renewable biomaterials are in the spotlight as a potential solution to increasing global greenhouse gas emissions. The construction industry contributes up to 40% of greenhouse gas emissions, with building materials responsible for a major portion. Research on high-performance materials with small carbon footprints has been steadily progressing. Wood is a sustainable building material with a high carbon fixation. Wood can be divided into the hard core and outer bark, both of which are very useful as building materials. In this study, a phase change material (PCM) was applied using vacuum impregnation to compensate for the poor thermal performance of wood. The thermal energy storage capacity of wood can be enhanced by applying aPCM, which has excellent latent heat/heat storage performance. The difference in the structural and chemical compositions of the core and bark of wood also has a significant influence onPCM impregnation. The thermal performance of shape-stabilized PCMs (SSPCMs) was evaluated by comparing the hierarchical structures and components of wood (core and bark). The PCM loading performance was verified by impregnation and surface/morphological property conversion analyses. When the porous structure of wood is filled with the PCM, its surface properties change from hydrophilic to hydrophobic. This was analyzed by contact angle measurements. The SSPCM with cork showed a 49% efficiency compared with the n-octadecane, which indicates an outstanding performance compared with other biomaterial-based PCM composites.

KEYWORDS

building materials, phase change materials, biomaterials, wood, cork, thermal energy

1 | INTRODUCTION

Renewable biomaterials have the potential to meet the growing global demand for energy and reduced greenhouse gas emissions.[1] The construction industry is considered as one of the most carbon-intensive industries, contributing up to 40% of total greenhouse gas emissions when the amount of carbon and energy consumed to operate buildings are considered.[2,3] In addition to operational carbon, the factors affecting the energy consumption of the construction industry include transportation, manufacturing, disposal, and building materials. In building and civil construction, raw materials extracted from the lithosphere account for 60% of the total raw material consumption.[4] Therefore, the development of sustainable building materials is essential to minimize

the industry's carbon footprint. Wood has suitable properties for applications in construction, such as renewability, high specific gravity and stiffness, light weight, fire resistance, excellent processability, and carbon storage capacity.[5] One cubic meter of wood can store approximately 1 ton of CO_2; hence, it has a huge carbon storage capacity and is the only building material that can have a positive impact on the environment.[6] Macroscopically, wood consists of a hard core, xylem, cambium, an outer layer, and bark. In this study, the hard part of the wood is referred to as the core. In the building filed, the core of wood can be used in buildings, furniture, flooring, and wall materials. Recently, the demand for wood has increased in response to more stringent environmental regulations, such as green and net zero carbon buildings.[7]

Balsa wood is a material with a very low specific gravity but high stiffness. It is a preferred building material, especially for sandwich panel cores. Vassilopoulos et al. produced balsa sandwich panels using a method that increased the anisotropy of the material.[8] They showed that the compression of balsa wood along the fiber direction significantly increased its energy-absorbing capacity owing to its porous microstructure. Borrega et al.[9] confirmed the presence of rays, vessels, and fibers in the cross-section of balsa wood by scanning electron microscopy (SEM). In the longitudinal section, balsa wood fibers were found to stand upright and gradual voids were observed.

Cork, a part of the harvested bark, is a protective layer made up of dead cells. In the wood industry, it is considered as a waste byproduct. Cork is regularly harvested (9-12 years), which allows the bark to grow naturally while helping the tree grow. The biggest feature of cork is its honeycomb structure. Wang et al.[10] found that the micro hexagonal structure of cork contains large pores of approximately 27 μm. As shown in Table 1, the chemical composition of cork is suberin (~50 wt.%), lignin (15-30 wt.%), polysaccharides (6-25 wt.%), and other extracts. Suberin is a material with an aromatic-aliphatic cross-linked polyester structure that constitutes the cell wall structure of cork.[11] Gallardo-Chacón et al. evaluated the potential of a material to adsorb volatile phenols using the chemical properties of suberin in cork.[12] As suberin has an aliphatic structure, it is advantageous because of its interaction with hydrophobic substances. As a type of low-carbon material, cork has excellent characteristics such as impermeability, durability, heat and sound insulation, and shock absorption. Cork is processed into chips of a certain size and used in various ways, for example, as a board for interior/exterior construction materials. Jorge et al.[13] concluded that cork insulation can improve the global warming potential (GWP); thus, it is helpful for GWP mitigation in most end-of-life scenarios. However, despite its environmental benefits, such as carbon storage and resource recycling, the thermal performance of wood core and bark makes it difficult to achieve the energy-saving goals required by the construction industry.

Phase change materials (PCMs) have a high latent heat density during the phase change process, such as solid–solid and solid-liquid; hence, they are utilized in thermal energy storage (TES) technology. The high latent heat of PCMs enables the efficient utilization of energy by accumulating and storing heat in the material during the phase change process, which can reduce building energy consumption. PCMs can be classified as inorganic, organic, and eutectic. Organic PCMs (eg, alkanes, polyethylene glycols, and paraffin waxes) are widely used because of their characteristics, such as a usable phase change temperature, high latent heat, excellent thermal and chemical stability, and almost no supercooling.[15] However, organic PCMs have disadvantages associated with liquid flow and leakage in the phase change temperature range. To address these problems, studies have been conducted on PCM stabilization techniques. To stabilize PCMs, researchers have focused on three methods: microencapsulation, macroencapsulation,[17] and shape-stabilized PCMs (SSPCMs). Various materials and methods have been studied for use in PCM containers. Researchers have considered the integration of PCMs by utilizing the eco-friendly and porous structure of wood. Fuentes-Sepúlveda et al.[18] impregnated Pinus radiata trees with n-octadecane using the Bethell method. The impregnated composite material showed a minimum and maximum latent heat enthalpies of 36 J/g and 122 J/g, respectively, depending on the orientation of the wood. Previous studies have attempted to improve the thermal performance of wood by applying PCMs.[19-22] Studies have shown that wood is suitable as a support material for stabilizing PCM. Cork is a material that must be recycled because it is classified as industrial waste. However, unlike wood core, few studies have been conducted on cork. Wood bark has a high utility value and potential as a future building material.

TABLE 1 Components of cork[14]

Cork(Q. suber)	Suberin	Lignin	Polysaccharides (cellulose and hemicellulose)	Extracts	Ash	Others
Component(%)	42.3	23.3	16.2	11.7	0.6	5.9

In this study, the potential TES capacity of wood, which can be observed during PCM impregnation, was evaluated by focusing on the differences in the structural and chemical properties of the wood core and bark. Figure 1 illustrates the research flow of this study. The structural differences between balsa and cork were observed by SEM and contact angle (CA) measurements. Fourier-transform infrared spectroscopy (FTIR) and energy-dispersive X-ray spectroscopy (EDS) were performed to directly confirm the different chemical

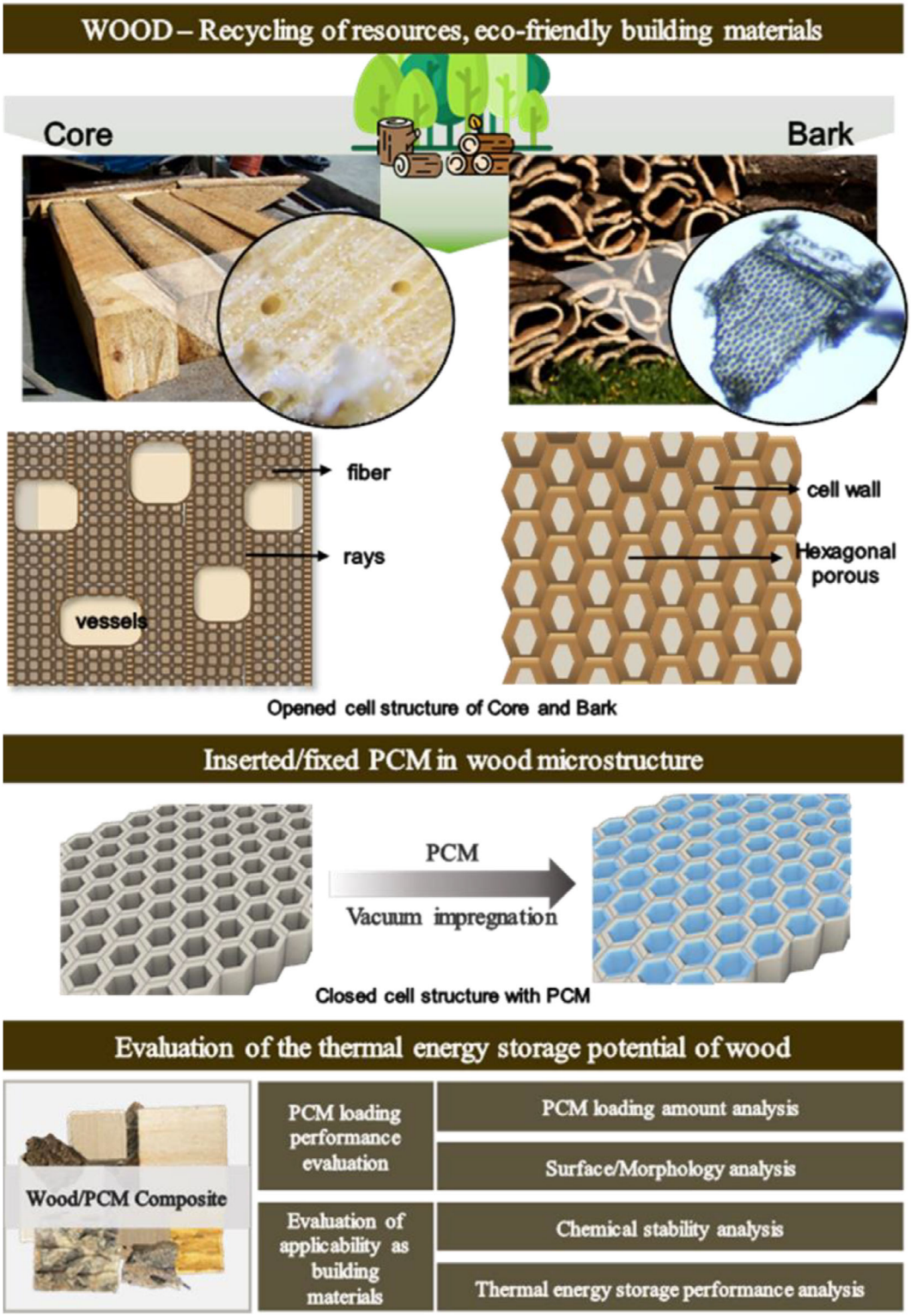

FIGURE 1 Research flow

compositions of balsa and cork. In addition, it was determined whether chemical bonds were formed between the wood and PCM during the SSPCM fabrication process. The chemical stability was evaluated to determine the availability of building materials. The compatibility with PCMs may vary depending on the structural/chemical characteristics of the material.[23] To prove this, PCM impregnation analysis was conducted through weight comparison and thermogravimetric analysis (TGA). The amount of impregnated PCM significantly affected the thermal performance of the SSPCM. The thermal performance was evaluated based on latent heat and thermal conductivity measurements. Finally, a leakage experiment was conducted to evaluate the thermal stability of the SSPCM. In this study, the PCM was impregnated into two materials: wood and cork. The heat storage performance of wood is improved, and then its thermal/morphological/chemical stability is evaluated. Finally, its potential applicability as a building material is discussed.

2 | MATERIALS AND EXPERIMENTAL METHODS

2.1 | Materials

In this study, balsa wood and cork were used as the matrix materials for PCM impregnation. Balsa wood (*Ochroma pyramidale [lagopus]*) was purchased from Balsanara in Korea. Balsa wood is native to the south-central regions of Brazil, Peru, and Ecuador. Figure 2 shows the cross-sectional and longitudinal sections of the balsa wood used in this study. The pores of balsa wood can be observed through the axial cross-sections in the growth direction of the wood. The macropore structure can be seen with the naked eye.

Cork (*Quercus variabilis Blume)* was sourced in Korea. Cork types can range from powder to chips depending on their size. To reflect this, the experiment was conducted by dividing the cork into large and small sizes; their thicknesses, however, were almost the same. Large cork particles have a width of at least 5 cm, while small particles have a width of less than 5 cm (Figure 2C, D). The difference in the amount of impregnated PCM could be observed depending on the specific surface area of the cork.

The phase change temperature suitable for practical applications in buildings is approximately 27°C-35°C.[24] In this study, an organic PCM, that is, n-octadecane (Celcious, Korea), corresponding to an appropriate phase change temperature range, was used. Several researchers have used n-octadecane as a PCM for building materials.[25] Table 2 summarizes the characteristics of n-octadecane.

TABLE 2 Physical properties of n-octadecane[26]

PCM	n-octadecane
Phase change temperature (°C)	18-38
Latent heat capacity (J/g)	256.5
Specific heat capacity (J/g·K)	92.0
Thermal conductivity (W/m·K)	0.26

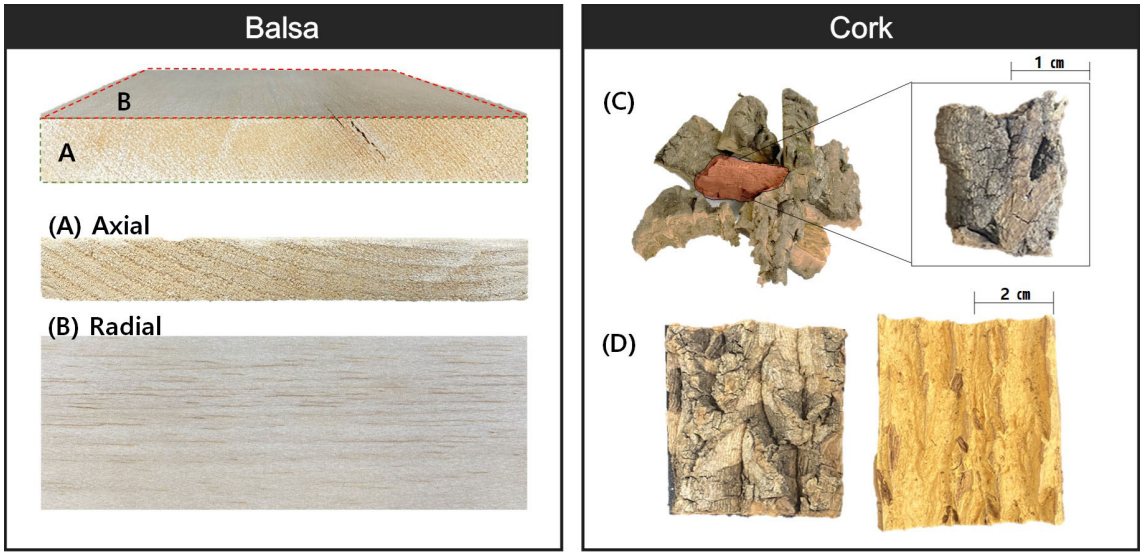

FIGURE 2 Core and bark of wood (balsa – (A) axial cross-section and (B) radial section; cork – (C) small particles and (D) big particles (front and backside)

2.2 | Fabrication process of SSPCM

PCM shape stabilization was performed using the vacuum impregnation method with balsa and cork as the support materials. When a vacuum is applied to a material with a porous structure, a negative pressure develops in the pores. The negative pressure enables the penetration of the PCM through capillary forces. When the vacuum is released, the PCM is absorbed into the pores by applying atmospheric pressure (101.35 kPa). The van der Waals force acting between the pore wall and PCM results in further stabilization. A three-step vacuum impregnation method (Figure 3) was performed to efficiently load the PCM with n-octadecane into the pores of balsa wood and cork. For various analyses and evaluations, large amounts of raw materials (small and large particles of balsa and cork) were prepared, as shown in Figure 2. Vacuum drying was performed to extract moisture from the prepared raw materials and the air in internal pores. The specimens were then placed in a vacuum oven and heated for 2 hours at a temperature of 110°C and a pressure of −0.085 kPa (Figure 3B). The conditions inside the oven were maintained in a vacuum state by a vacuum pump. The primary vacuum heating treatment increased the PCM impregnation potential by removing the air and moisture in the porous structure of the raw materials. After the first treatment, n-octadecane was added at 30°C to submerge the raw materials and achieve a high PCM impregnation. The PCM ratio is the amount required to completely submerge the raw material. The weight ratio of the PCM and raw material is approximately 2:1. At this time, buoyancy was generated in the specimens owing to the high density of the PCM. Buoyancy caused the specimens to float to the PCM surface,

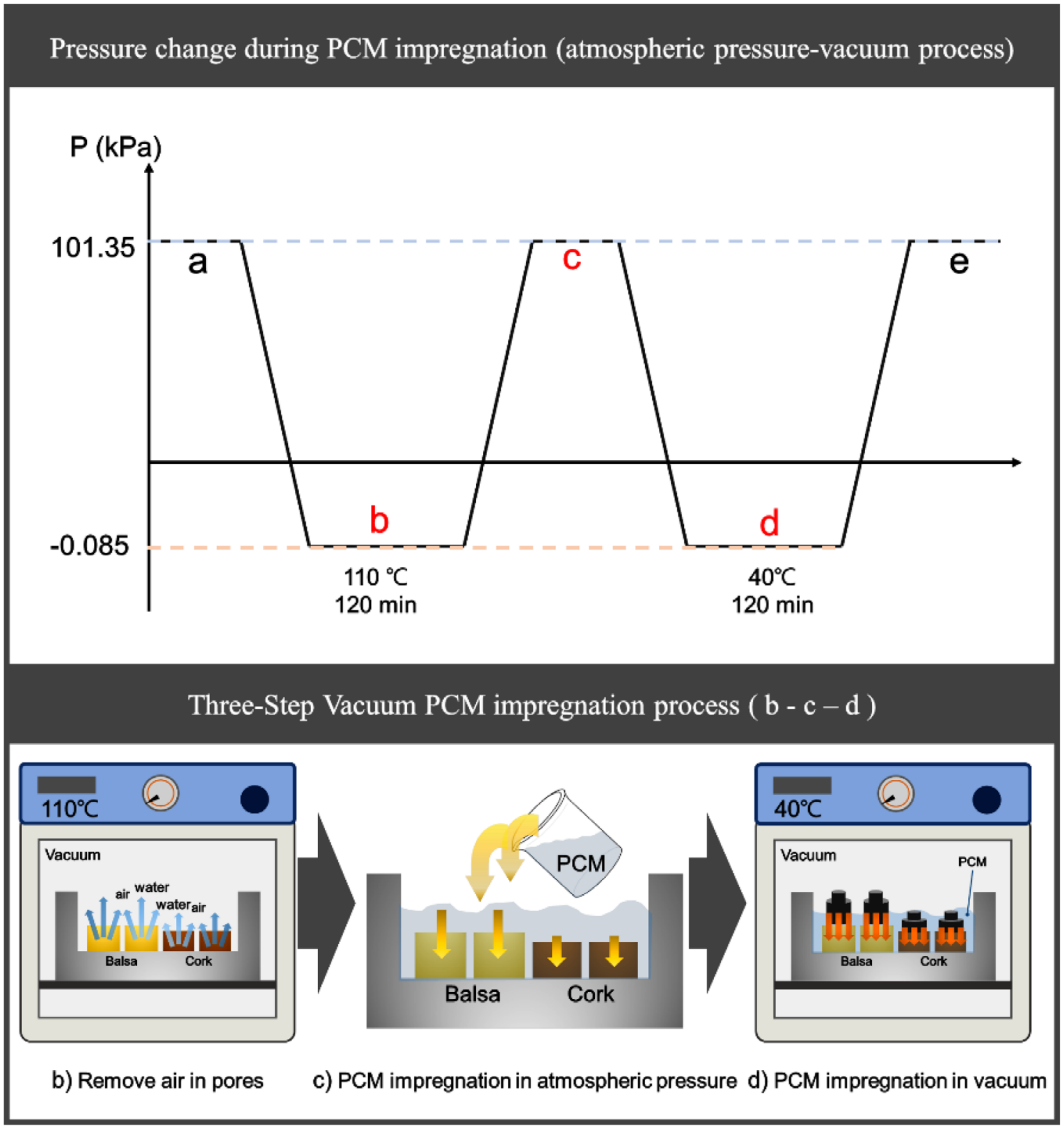

FIGURE 3 SSPCM fabrication process. (A) atmosphere, (B) remove air in pores using a vacuum oven, (C) PCM impregnation in atmospheric pressure, (D) PCM impregnation in vacuum, and (E) filtering

preventing impregnation on all sides of the specimen. To solve this problem, a weight of 5 to 7 g was applied to submerge the specimen in the PCM. Impregnation under atmospheric pressure was carried out for approximately 15 minutes, and then the second vacuum impregnation process was performed. Vacuum impregnation was carried out for 2 hours at 40°C and −0.085 kPa in a vacuum oven (Figure 3C). After the second vacuum impregnation, a microfiber cloth was used to remove the PCM from the surface of the specimen. The final products, that is, the balsa wood/PCM composite was named Balsa_oct, while the cork/PCM composite was named Cork_oct.

2.3 | Characterization techniques

2.3.1 | Surface/morphological analysis

Morphological analysis of the presence of PCM in the microstructure of the porous material was performed using field-emission SEM (FE-SEM). The microstructures of the specimens were photographed at various magnifications. The FE-SEM analysis was performed by applying an acceleration voltage of 15 kV at room temperature. The specimens were coated with gold (Au) to prevent distortion by electron beams. The hydrophilicity/hydrophobicity of the SSPCM surface was analyzed by measuring the CA. The raw material (balsa) is hydrophilic with a high water absorption capacity. In contrast, cork is a hydrophobic material because of the hydrophobic component, suberin. n-Octadecane is an organic PCM and an oily hydrophobic material.[27] Therefore, when the PCM was successfully impregnated into the pores of balsa and cork, the wood/PCM composites have a stronger hydrophobicity than before impregnation. The contact angle measurement (MSA, KRUSS corp., Germany) was used to measure the CA between the droplet and specimen. It has a dosing system with a 2-fold liquid needle and a camera with a resolution of 1000 × 700 pixels. The specimen was placed on the measuring table with a three-axis stage. The position of the fixed camera was adjusted and a droplet was released to measure the CA between the specimen and droplet. The CA is defined as the angle between the solid surface and tangent drawn on the falling surface and passed by the atmosphere-liquid-solid triple point. The advancing angle, which is the CA generated by the expansion of liquid, was determined using the ADVANCE software. The change in the CA of the droplet was caused by an electric force acting on the three-phase contact line.[27] Figure 4 shows a schematic diagram of the changing CA as the internal pores were filled during the PCM impregnation process. Wood cells with a porous structure exhibit excellent water absorption. By filling the pores with the PCM, the surface of wood cells has low water absorption and hydrophobicity, which can be analyzed by CA measurements. In other words, CA analysis enables the observation of the hydrophobic properties affected by PCM impregnation.

2.3.2 | Evaluation of the chemical stability of SSPCMs

An analysis was performed to confirm the formation or disappearance of chemical bonds between the balsa, cork, and PCM during PCM impregnation. The FTIR peak table can be used to determine the chemical bonds between the elements present in the SSPCM through peak values. The chemical stability of SSPCMs can be evaluated by analyzing the chemical bonding of the materials before and after PCM impregnation. FTIR (VERTEX 80v/HYPERION 2000, Bruker Corp.) measurements were performed in the wavelength range of 4000 to 600 cm^{-1}. The chemical bonds were analyzed by comparing the FTIR and EDS results. EDS is an analysis technique that enables the rapid qualitative analysis of elements.

2.3.3 | PCM loading amount analysis

To analyze the possibility of PCM impregnation into the wood material, a weight comparison, TGA, and SEM

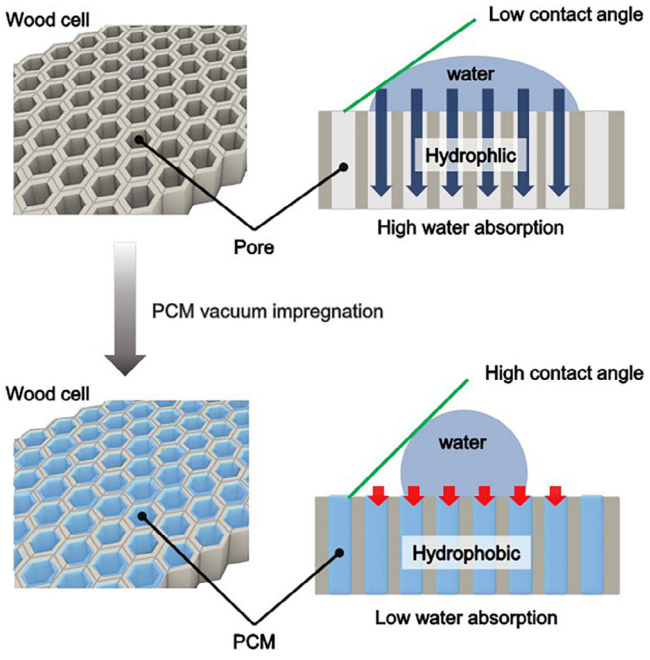

FIGURE 4 Schematic of wood cell surface properties changed by PCM impregnation

were performed. Before PCM impregnation, the total dry weight of all specimens (110°C, vacuum oven-dried for 2 hours) was measured. The weight before PCM impregnation is expressed as W_{bpi} in Equation (1). After PCM impregnation and filtration, the weight of the specimen W_{api} was measured and substituted into Equation (1) for analysis. At the macro level, the weight gain rate was used to determine whether the PCM was fixed to the internal pores of the wood.

The amount of PCM impregnation, loading performance, and thermal stability were also analyzed by TGA (Discovery; TA Instruments) in accordance with the ASTM E 1582-17[28] standard test method for the temperature calibration of thermogravimetric analyzers. The PCM container materials (balsa, cork) and fabricated SSPCMs (Balsa_oct and Cork_oct) were heated from 0°C to 600°C at a rate of 10°C/min in a nitrogen atmosphere.

$$\text{Weight gain rate} = \frac{W_{api}\text{-}W_{bpi}}{W_{bpi}} \times 100\%, \quad W_{api}: \text{Dry weight after PCM impregnation}, \quad W_{bpi}: \text{Dry weight before PCM impregnation}. \tag{1}$$

2.3.4 | Thermal performance analysis of SSPCMs

The SSPCMs (Balsa_oct and Cork_oct) are expected to have improved thermal performance compared with the raw materials. Latent heat and thermal conductivity analyses were conducted to evaluate the thermal capability of the PCM. The PCM exhibited a high latent heat during the phase change process. Both Balsa_oct and Cork_oct also exhibited the high latent heat characteristics of the PCM. Latent heat analysis was performed using a differential scanning calorimeter (Discovery DSC; TA Instruments). The analysis was carried out at the temperature increase rate of 10°C/min in a nitrogen atmosphere. In addition, the temperature section was carried out at 0°C to 60°C, including the phase change section of n-octadecane. The enthalpy was derived from the calculated latent heat. The thermal conductivity was analyzed using the HFM method for balsa and Balsa_oct, and the laser/light flash method (LFA) for cork and Cork_oct. The balsa was machined to a size of 110 mm × 110 mm × 20 mm (W × D × H). Thermal conductivity measurements were performed using the HFM 446 (NETZSCH) according to the ASTM C518[29] standard test method. When the thermal equilibrium was realized, the thermal conductivity of the HFM was calculated by measuring the temperature gradient at a temperature difference of 20 K between the hot and cold plates. To obtain the accurate thermal conductivity, the mean temperatures were set as 25°C and 40°C for each specimen three times. Cork and Cork_oct were prepared as power-type specimens, and their thermal diffusivities were measured using the LFA 427 apparatus (NETZSCH). The analysis was performed according to ASTM E1461-13[30] standard test method. The thermal conductivity was calculated based on the measured data.

2.3.5 | Evaluation of PCM leakage stability according to temperature change

The PCM leak stability was considered in the SSPCM performance evaluation. As the PCM was stably loaded, the thermal storage performance of the SSPCM remained constant regardless of the external temperature changes. An experiment was performed to characterize the PCM leakage. First, the raw materials (balsa and cork) were prepared as controls for comparison with the SSPCM. The raw materials and SSPCM were combined on filter paper, and placed in a vacuum oven at a temperature of 50°C. The leakage of the SSPCM specimen was confirmed by observing the filter paper at intervals of 2 hours.

3 | RESULTS AND DISCUSSION

3.1 | Morphological and surface analysis of SSPCMs

3.1.1 | Observation of impregnated PCM in porous structure

The microstructural changes caused by PCM impregnation into the porous material were observed through SEM analysis. Figure 5 shows the microstructures of balsa, cork, Balsa_oct, and Cork_oct. Wood fiber structures, rays, and vessels were observed in the balsa (Figure 5A,A-1). In the cork (Figure 5C,C-1), a characteristic porous honeycomb structure was observed, and 500x and 1000x magnifications were obtained for all specimens. Figure 5B,B-1,D,D-1 show the SEM analysis results for Balsa_oct and Cork_oct. Figure 5A,A-1 show the presence of vessels and fibers in the balsa microstructure. The maximum pore size of the vessel is 23.15 μm, while the fiber structure is entangled, resulting in a dense image. Figure 5C,C-1 show the internal porous structure of the cork. Compared with balsa, a large number of pores and a honeycomb structure were observed. The pore sizes ranged from approximately 19.76 to 49.76 μm. It was confirmed that balsa and cork are porous materials with hierarchical distributions of pore sizes. In the case of

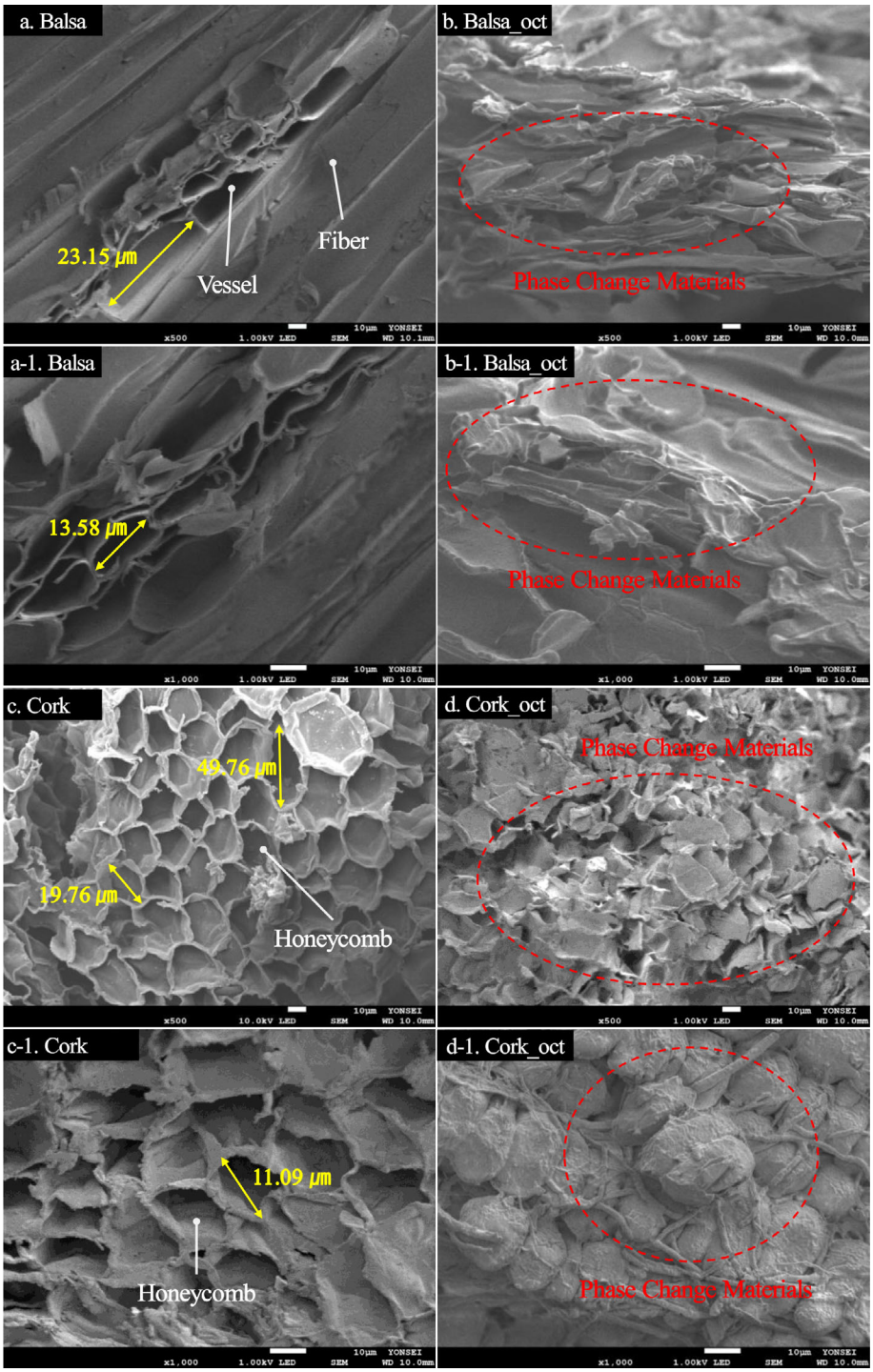

FIGURE 5 SEM images of the microstructure morphology before and after PCM impregnation

Balsa_oct (Figure 5B,B-1), a rough surface that was not present before PCM impregnation was confirmed, and a vessel filled with PCM was observed. Cork_oct (Figure 5D,D-1) showed a morphological change in which the PCM filled the honeycomb structure. SEM analysis confirmed that the PCM was successfully immobilized in the porous structure. Morphological changes occurred owing to the fixation of the PCM in the internal pores of balsa and cork. In particular, PCM impregnation into the porous structure facing the external surface and the PCM remaining on the rough surface can change the properties of the specimen.

3.1.2 | Analysis of wood surface properties by impregnating PCM

The conversion of the surface properties and wettability of the material during PCM impregnation was analyzed by CA measurements. n-Octadecane is hydrophobic

rather than hydrophilic, which is a characteristic that can occur in the fabricated SSPCMs. To confirm the surface characteristics and wettability by moisture, CA measurements were performed according to the ASTM D 5946 and ASTM D 7334-08 to characterize the wettability of the surface. The CA measurement results are presented in Table 3 and Figure 6. Table 3 lists the CAs of the droplet on measured on the left, right, and both sides. The images in Figure 6 were taken at the same time point immediately after the droplet was dropped onto the surface. Balsa is a highly hydrophilic material. Because of its high water absorption rate, water was absorbed before the CA measurement was performed, resulting in large measurement errors. In Figure 6, the CAs of balsa are approximately 45.3° and 14.7°, while those of Balsa_oct are approximately 122.6° and 120.7°. According to ASTM D7334-08,[31] which characterizes the surface wettability, balsa is hydrophilic and Balsa_oct is hydrophobic. It can be seen that the organic PCM penetrated the balsa pores, was impregnated, and changed the hydrophilic characteristics of the material to hydrophobic.

3.2 | Evaluation of the chemical stability of SSPCM

FTIR spectroscopy measurements were used to evaluate the chemical compatibility and stability during the integration of the balsa, cork, and PCM (Figure 7). EDS mapping was performed to compare the FTIR results with

TABLE 3 The contact angle of the droplet measured on the sample surface (left, right, both sides)

	Average CA		
Specimen	**Left side (°)**	**Right side (°)**	**Both side (°)**
Balsa	74.71 (±41.61)	59.74 (±63.75)	67.22 (±52.68)
Balsa_oct	128.48 (±5.38)	129.72 (±5.25)	129.10 (±5.32)
Cork	116.00 (±9.28)	116.17 (±6.34)	116.09 (±7.81)
Cork_oct	129.92 (±6.52)	133.7 (±5.11)	131.81 (±6.78)

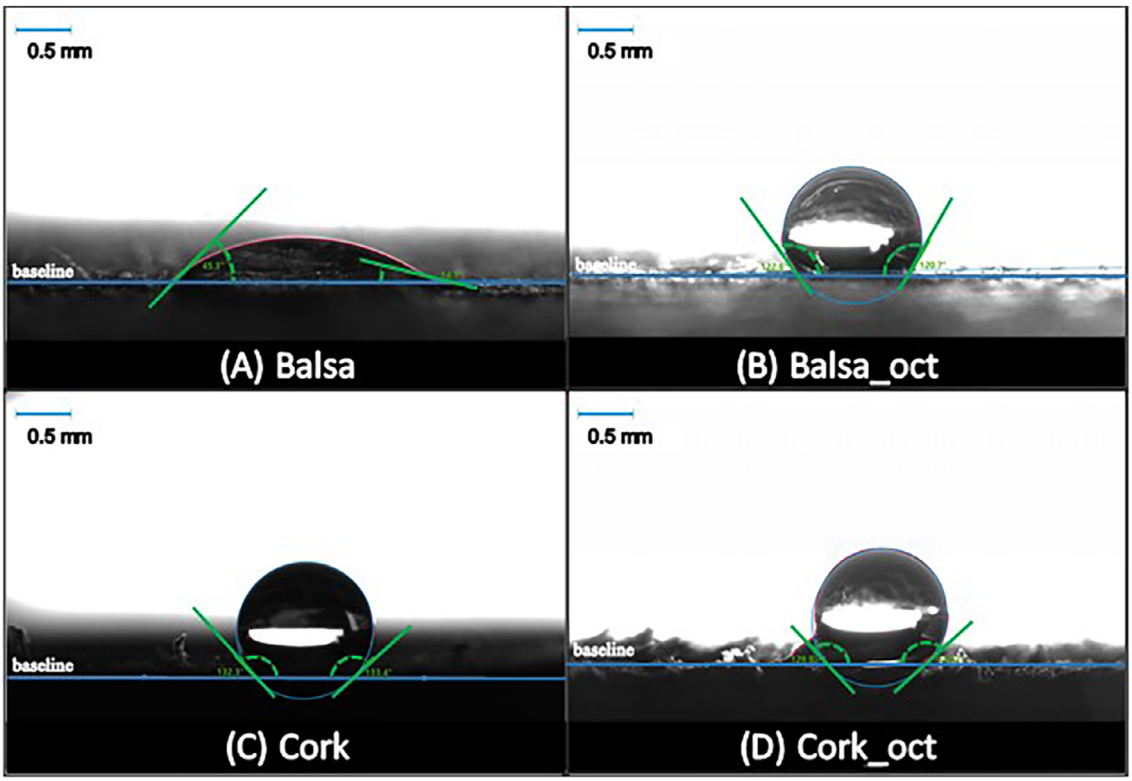

FIGURE 6 Changes in the contact angle of the wood surface according to the PCM impregnation

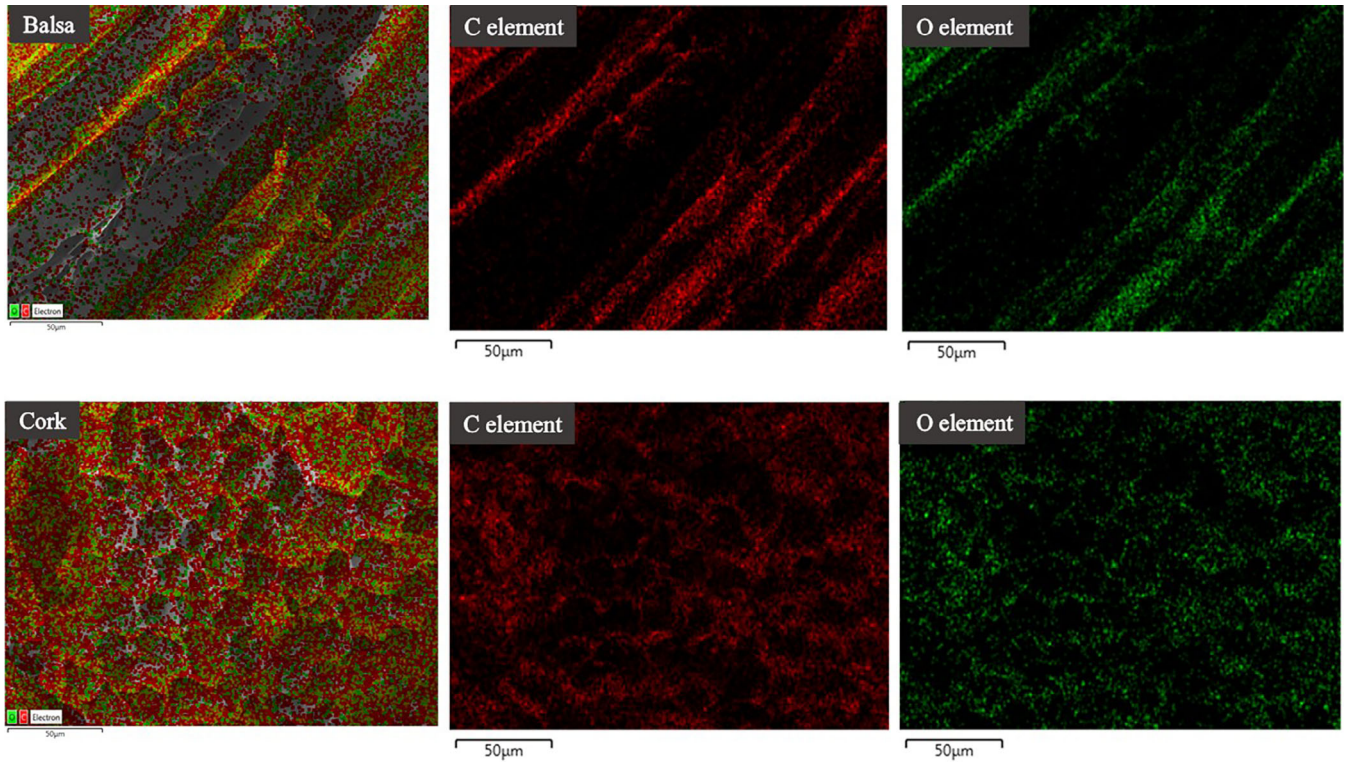

FIGURE 7 EDS mapping images of the carbon and oxygen distribution of balsa and cork

those of actual wood components. Figure 8 shows the FTIR transmission spectra of balsa/Balsa_oct and cork/Cork_oct. The chemical components of wood include carbon, hydrogen, oxygen, and nitrogen. The chemical elements in balsa and cork can be inferred from the EDS mapping images (Figure 7). The actual carbon and oxygen distributions can be confirmed in the balsa and cork element distribution images (Figure 7) and element distribution characteristics (Table 4). The hydrogen element could not be traced in the EDS mapping analysis.

The representative components of wood: cellulose, hemicellulose, lignin, and polysaccharides, have CC, CH, and CO bonds. In the FTIR graph (Figure 8), many peak values were observed owing to various stretching and bending vibrations of various chemical bonds. Spectral analyses of balsa and Balsa_oct are shown in Figure 8. The characteristic spectral peak observed in the existing balsa tree appeared at 1029 cm^{-1}. The peak value represents the COC symmetric stretching and CO stretching of cellulose and hemicellulose in balsa wood. The transmission spectrum of Balsa_oct showed various peak values at 1030 to 800 cm^{-1}. This behavior is similar to the peak values of balsa and is attributed to the COC symmetric stretching in pyranose rings and CO stretching in the aliphatic groups of cellulose hemicellulose. The large peak value in the SSPCM is caused by the existing cellulose and hemicellulose components and the C-H alkyne present in the PCM. The chemical bonds corresponding to the characteristic peaks that appear only in SSPCMs are described in the graph. This is a peak for a specific bond that occurs in n-octadecane. The detailed wavelength section in Table 5 presents the results of the FTIR analysis of cork/Cork_oct. The peak patterns of cellulose, hemicellulose, and lignin—the same components as in balsa—are shown. A peak was observed at 1562 cm^{-1}, which is in the wavelength range of the carbonyl group corresponding to the chemical structure of suberin, the main component of cork. The coincident peak wave range occurred before and after PCM impregnation, suggesting that the composition of suberin was maintained. This was frequently observed before and after PCM impregnation. The wave transmission range (3200-2600 cm^{-1}) corresponding to suberin can be evaluated only in cork and Cork_oct. As a component that does not exist in balsa, CH symmetric stretching and OH bending of suberin were observed. The peak values of the chemical bonds corresponding to the wood components (cellulose and hemicellulose) of balsa and the suberin component of cork were derived through FTIR analysis. The peak table analysis of SSPCMs (Balsa_oct and Cork_oct) confirmed the peak data corresponding to the PCM and raw materials. It

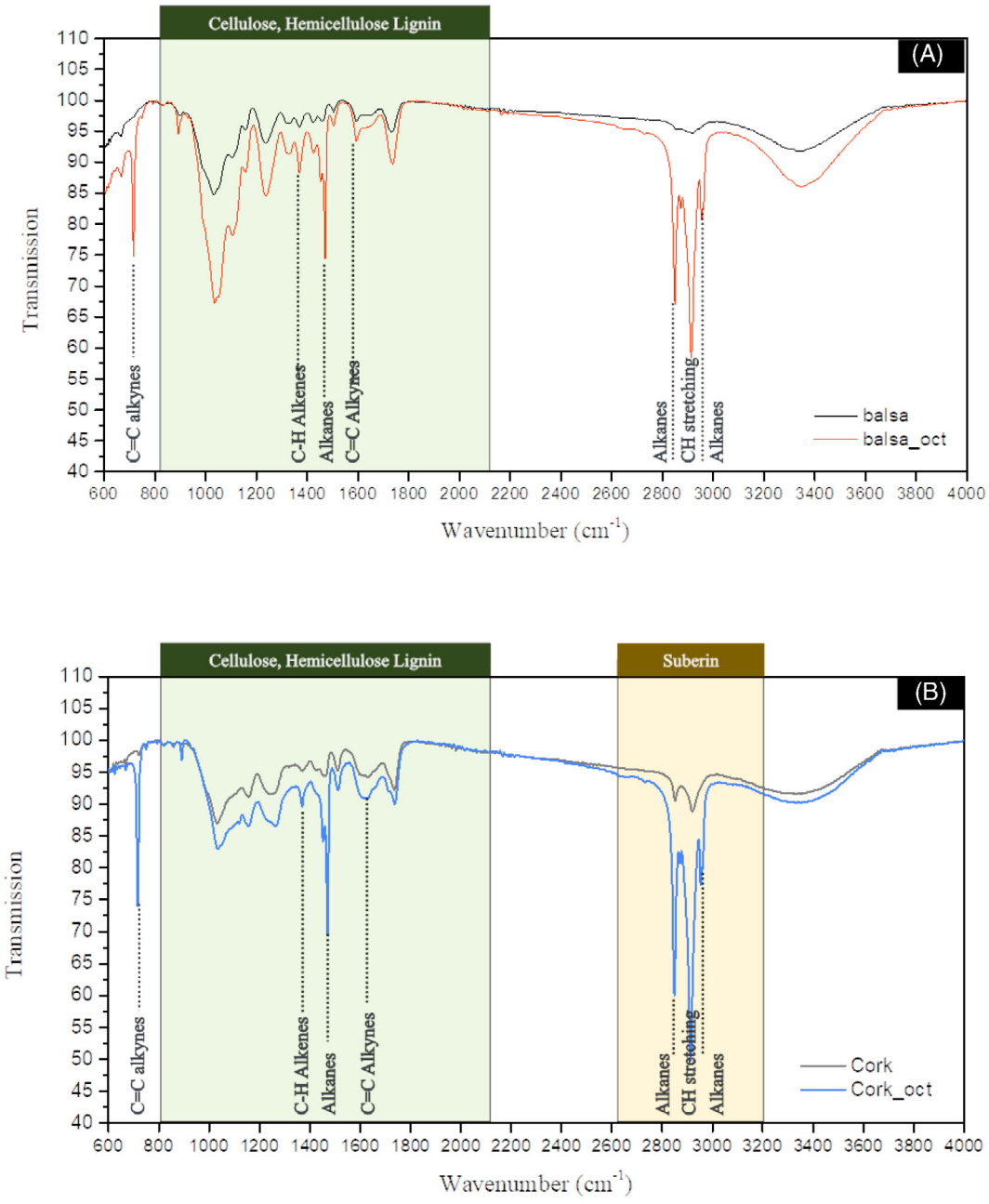

FIGURE 8 FTIR transmission peak. (A) balsa and Balsa_oct; (B) cork and Cork_oct

TABLE 4 EDS element analysis results of balsa and cork

	Balsa		Cork	
Element	**Wt.%**	**Atomic %**	**Wt.%**	**Atomic %**
C	60.03	66.67	77.01	81.69
O	39.97	33.33	22.99	18.31
Total	100.00	100.00	100.00	100.00

was also confirmed that no chemical reaction occurred between n-octadecane and the supporting materials during PCM impregnation.

3.3 | Analysis of PCM impregnation by the difference between porous structure and components

3.3.1 | Weight comparison analysis in PCM impregnation process

A weight comparison was performed to analyze the PCM absorption properties of balsa and cork. In the SSPCM fabrication process, weights were applied to all specimens to counter the buoyancy caused by the high density of the PCM. Several raw materials were prepared to

TABLE 5 Frequency according to chemical band assignment

Components	Band assignments	Frequency (cm^{-1})
Cellulose	CH_2 rocking vibration	1320
	CN stretching, OH	1333
	CH stretching (methyl and methylene groups)	2922
	hydrogen bonding (Inter and intra-molecular)	3337
Cellulose hemicellulose	COC symmetric stretching in pyranose rings CO stretching in aliphatic groups	1020
Cellulose Lignin	CO stretching	1642
Cellulose Lignin	Absorbed OH bending vibrations CO stretching conjugated to the aromatic ring	1370
Cellulose, Hemicellulose	CH deformation Aliphatic CH stretching in phenol and methyl group	895
Cellulose, Hemicellulose, Lignin	CH stretching out of the plane of the aromatic ring of glucose guaiacyl ring.	808
Hemicellulose, Lignin	CO stretching in carbonyl (unconjugated ketone and aliphatic groups xylan) CO vibration (in ketones, and aldehydes in hemicellulose) Esters (in lignin).	1740-1730
Lignin	COC stretching of phenol-ether bond in lignin	1233
	Stretching of the guaiacyl ring and OCO; CO stretching in lignin	1263
	Aromatic skeletal vibration typical for S units plus CO stretch	1594
	CO stretching, CC aromatic cycles in syringyl units	1611
	CC stretching in the aromatic cycle; aromatic skeletal vibrations in guaiacyl rings	1510-1505
Polysaccharide	Ring asymmetric valence vibration	1105
Suberin	CH asymmetric bending	1469-1438
	CH bending	
	CH symmetric stretching	2850
	OH bending	3340
	CO carbonyl group	1562
PCM	Alkanes	2960-2850
		1470-1350
	C–H alkenes	1400-1380
		3080-3020
	C–H alkynes	1000-675
		3330-3267
	C=C alkenes	700-610
	C=C alkynes	1680-1640
	CH3-umbrella deformation	2260-2100

consider these variables (Figure S1). The weight measurements were conducted three times. The SD in all measurements was approximately zero. The average dry weights of balsa, cork, and SSPCMs are listed in Table S1.

Figure 9 shows that the SSPCM impregnated with n-octadecane had a minimum and maximum weight increase 20.79% and 47.28%, respectively. The balsa specimens showed a weight increase of over 40%, whereas the cork specimens showed a weight increase of 20%-47%. The large deviation between the results of the cork specimens is attributed to the buoyancy action. In the vacuum impregnation process, specimen F floated to the PCM

surface owing to the weight deviation. In addition, the buoyancy of corks C and D exceeded their weights and floated. Thus, corks C, D, and G were not impregnated on all sides, resulting in their low weight gain. The average weight increase of the specimens, excluding impregnation, was 42.96%, 42.17%, and 46.65% for Balsa_oct, Cork_oct, and the total SSPCM, respectively. In the weight comparison analysis, the weight of the SSPCM after filtration and drying was compared with that before impregnation. In all cases, a weight increase was observed. Thus, it can be inferred that a smooth PCM impregnation was performed.

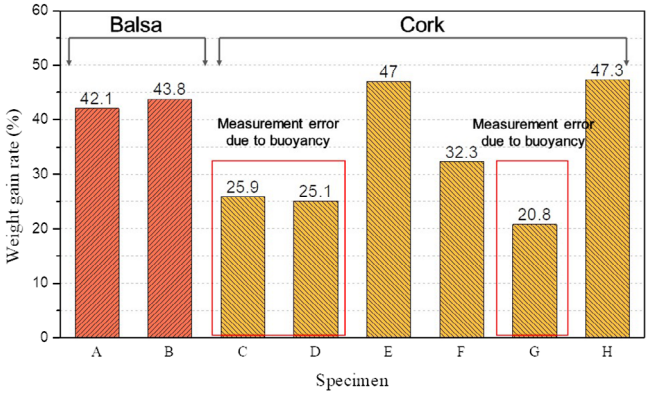

FIGURE 9 Comparison of weight gain rate of balsa and cork after PCM impregnation

3.3.2 | Analysis of PCM impregnation rate according to pyrolysis temperature of SSPCM

The proportion of PCM in the SSPCM was analyzed by measuring the oxidation rate according to the pyrolysis temperature of the material. The TGA and derivative thermogravimetric (DTG) (derived weight [%/°C]) results of the SSPCM-based wood are shown in Figure 10. The

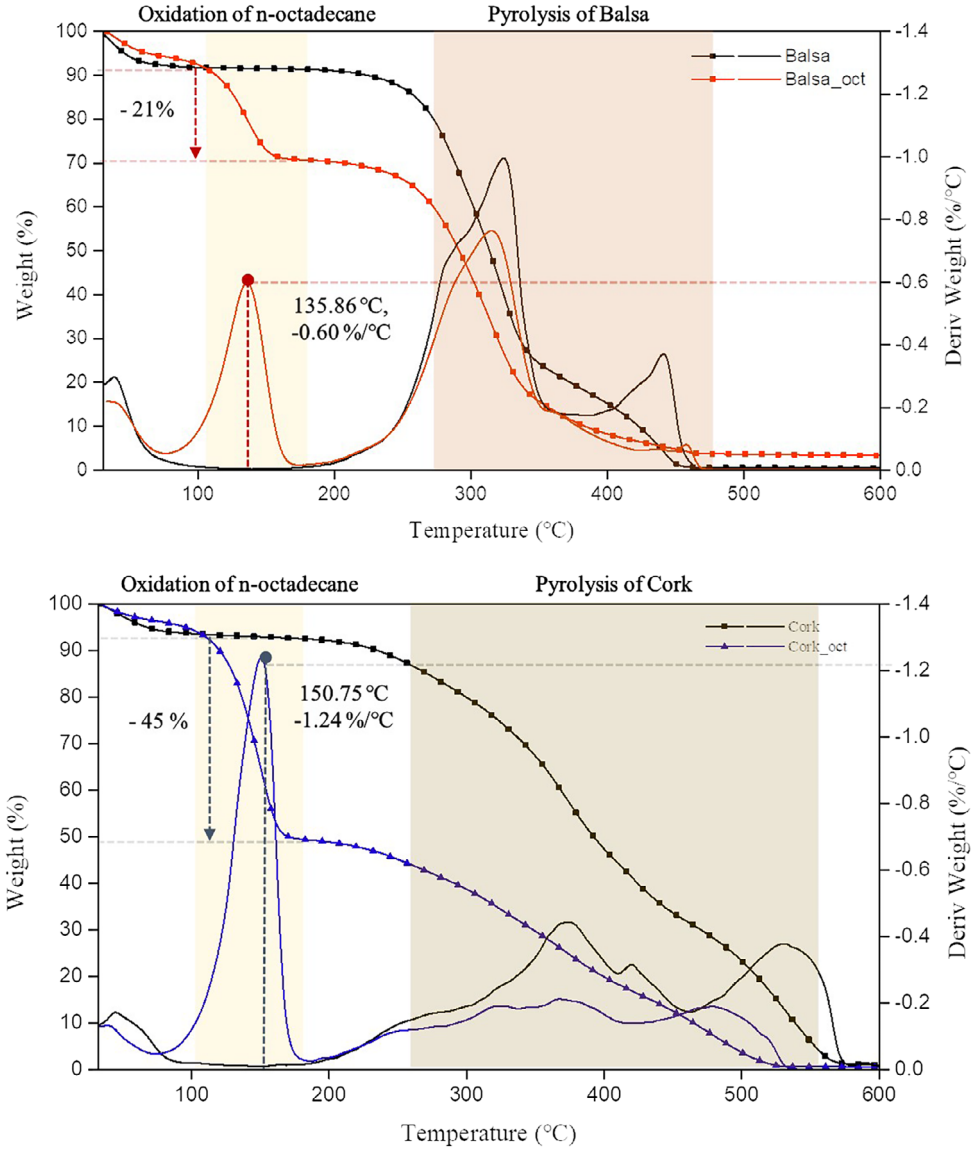

FIGURE 10 Thermogravimetric curves for the quantitative analysis of impregnated PCM

organic PCM (n-octadecane) has a pure alkane chain consisting of carbon and hydrogen. The oxidation temperature was approximately 130°C to 170°C. As seen in the figure, balsa wood was compared with impregnated balsa and SSPCM. Two large weight losses were observed in the balsa TGA curve. When the graph of impregnated Balsa_oct was analyzed, the weight loss was large at 130°C to 170°C. Weight loss was not observed in balsa with the Balsa_oct SSPCM. This implies that the PCM was impregnated. In the PCM oxidation temperature range, the DTG curve of Balsa_oct showed a weight loss rate of 0.60%/°C at 135.86°C. The weight loss rate increased during the thermal decomposition of balsa. Balsa contains the wood components cellulose, hemicellulose, and lignin. The DTG peak at 250°C to 350°C appeared to be the same in balsa and Balsa_oct because of the thermal decomposition properties of the wood components. The PCM oxidation rate was lower than that of the wood components. Therefore, Balsa_oct was impregnated with PCM, but the amount of PCM was relatively smaller than that of the wood components. In the TGA graph of cork and Cork_oct, the cork curve showed a gentle slope at over 300°C and a weight reduction. Cork_oct showed a weight reduction of approximately 45% in the oxidation temperature range of n-octadecane after the initial weight loss due to water removal. The DTG curve of Cork_oct showed a weight loss rate of 1.24%/°C at 150.75°C. Unlike Balsa_oct, it exhibited the largest peak value in the PCM oxidation temperature range over the entire temperature range. After the large weight loss of the PCM, the pyrolysis of wood components proceeded with a gentle slope. This means that the PCM accounts for a large amount of the total weight. It can be concluded that Cork_oct has a larger amount of PCM impregnation than Balsa_oct. Thus, the characteristic structure of cork influenced the PCM impregnation. The hydrophobicity of cork, regular arrangement of hexagons, and large specific surface area are advantageous for PCM impregnation. In addition, balsa wood, cork, Balsa_oct, and Cork_oct showed little change in weight at over 500°C; thus, the weight loss (%) converged to zero. It can be seen that the raw materials and SSPCMs have high thermal stability.

3.4 | Thermal performance of SSPCM analysis

3.4.1 | Heat storage capacity analysis

Figure 11A,B show the DSC curves of the melt-freezing process of the PCM container materials and SSPCMs. No peak values were observed in balsa or cork. It is possible to analyze the latent heat of a material using the peak in the DSC curve and its integral value. The fact that peaks not found in the raw materials (balsa and cork) were found in the SSPCMs (Balsa_oct and Cork_oct) means that the PCM impregnation process was successful. Thermal properties, including melting temperature (T_m), freezing temperature (T_f), and enthalpy (ΔH_f) are listed in Table 6. Balsa_oct showed major melt-freeze transition

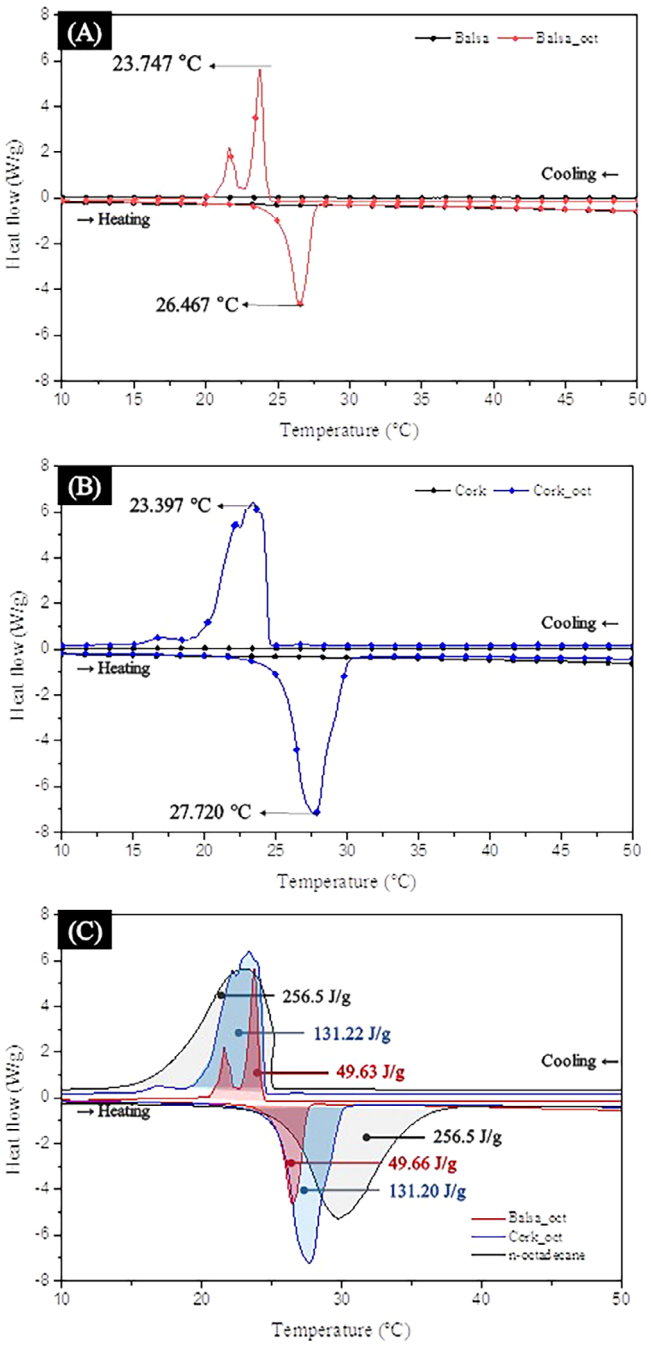

FIGURE 11 Comparison of peak temperature and latent heat by DSC curve analysis. (A) balsa and Balsa_oct; (B) cork and Cork_oct; and (C) n-octadecane and SSPCMs

TABLE 6 n-Octadecane and SSPCM thermal properties

Specimen	Melting temperature (°C)	Freezing temperature (°C)	Latent heat	
			Liquid–solid melting (J/g)	Liquid–solid freezing (J/g)
n-octadecane	29.765	23.171	180.75	184.83
Balsa_oct	26.467	23.747	49.66	49.63
Cork_oct	27.720	23.397	131.20	131.22

temperature peaks at 26.467°C and 23.747°C, respectively. This is similar to the phase transition behavior of the raw PCM, indicating the stable integration of the PCM into the balsa.

In the case of Cork_oct, the melting and freezing temperatures were 27.720°C and 23.397°C, respectively. All SSPCMs showed peaks in the phase change section of the raw PCM. In the PCM phase transition region, the heat storage capacity of Balsa_oct is 49.66 J/g and 49.63 J/g, which is approximately 20.75% of the performance of n-octadecane. Cork_oct had latent heat values of 131.20 and 131.22 J/g and exhibited 54.35% of the performance of raw PCM. Cork_oct exhibited excellent melting-freezing temperature behavior and heat storage capacity. The difference in latent heat between Cork_oct and Balsa_oct is attributed to structural/chemical differences (Sections 3.1 and 3.2). The characteristic honeycomb structure of cork works well when impregnated with a PCM. The capillary force between the hexagonal face and PCM holds the integrated PCM. The chemical compatibility between the PCM and support materials plays an important role in the SSPCM fabrication process.[32] FTIR and EDS confirmed the presence of the hydrophobic substance, suberin, in cork. Owing to suberin, Cork_oct had a high interface performance. DSC analysis confirmed the excellent latent heat performance and heat storage capacity of Cork_ oct. Balsa_oct showed similar behavior as the PCM, and exhibited a thermal performance that did not exist in balsa. The PCM properties can be attributed to the physical bonding of the PCM inside the balsa and cork. It is suggested that the phase stabilization method of the PCM through balsa and cork can be helpful in practical applications. The enthalpies of the SSPCMs in previous studies prepared using PCMs with a phase change temperature similar to that of n-octadecane were compared (Table 7). Table 7 lists the peak temperature and enthalpy of SSPCMs based on biomaterials such as wood; mineral SSPCMs with the same porous materials but not biomaterials; and SSPCMs based on carbon materials that were recently considered owing to their porosity and high thermal conductivity. Recently, research on carbon-based SSPCM fabrication has been actively conducted to improve the thermal storage efficiency of PCMs. SSPCMs using porous carbon as the PCM container material have enthalpies in the range of 85 to 196 J/g, indicating a high thermal storage performance. However, these have a relatively low latent heat compared with biomaterial/PCM composites similar to wood. In this study, the PCM containers (balsa and cork) show an above-average latent calorific value and excellent thermal performance among biocomposites.

3.4.2 | Thermal conductivity analysis for PCM performance improvement analysis

Figure 12 shows the thermal conductivities of SSPCMs made of wood, PCM, and n-octadecane. Thermal conductivity analysis was performed at 20°C to 40°C, including the phase change region of n-octadecane. The analysis was repeated three times and had an average SD of 0.00536. Figure 12 shows the analysis results of the average thermal conductivity at room temperature and 40°C. Air has excellent thermal insulation performance; thus, balsa and cork with hierarchical porous structures have low thermal conductivity. The thermal conductivity of n-octadecane is approximately 0.184 W/mK. Balsa_oct and Cork_oct showed higher values than the PCM. Because the thermal conductivity of air is much lower than that of the PCM, the thermal conductivity of Balsa_oct and Cork_oct increased as voids were replaced by the PCM. In the case of Balsa_oct, the thermal conductivity showed a slight increase according to the impregnation. Compared with n-octadecane, the thermal conductivity of Cork_oct improved by approximately 114%. Unlike Balsa_oct, the thermal conductivity of Cork_oct significantly improved. As the temperature increased, various processes occurred inside the material. Solid molecules exhibit enhanced thermal motion to promote fluid convection heat transfer in the voids as well as heat conduction in the solid skeleton. The radiant heat transfer between the pore wall and the wall also improved, thereby increasing thermal conductivity.[42] In the case of cork, the presence of a larger number of pores compared

TABLE 7 Comparison of SSPCM thermal performance in previous research

Category	Container material	PCM	Phase change temperature	Process	Peak temperature (°C)	Enthalpy (J/g)	Ref.
Carbon	XGnP	n-octadecane	28	melting	24.8	104.5	[33]
				cooling	31.13	110.9	
	Activated carbon (AC)		27–35	–	–	118.5	[34]
				–	–	113	
	Expanded graphite			–	–	196.8	
				–	–	196.3	
	XGnP			–	–	112.4	
				–	–	110.8	
	Polystyrene/ expanded graphite			melting	31.38	84.78	[35]
	TiO_2	n-octadecane 30 wt.%	27–35	melting	27.8	44.2	[36]
				cooling	26.9	43.7	
		n-octadecane 50 wt.%		melting	27.9	85.8	
				cooling	26.8	82.5	
Mineral	Expanded perlite	n-octadecane	27–35	-	-	128.5	[37]
	Expanded vermiculite			-	-	87.2	
	Nano size bentonite			melting	27.39	47.31	[23]
				cooling	24.18	47.32	
	Organic modified nanocly (Closite 20)			melting	28.89	113.1	
				cooling	22.88	95.05	
Biomaterials	Delignified wood	capric acid palmitic acid	23.4			94.4	[38]
	Pinus wood	PEG800 70 wt. %	25.2	melting	25.6	14.1	[39]
				cooling	16	11.6	
	Wood fiber	capric acid-stearic acid 25 wt.%	19-26	melting	24.23	44.5	[40]
				cooling	20.24	44.1	
		capric acid-stearic acid 50 wt.%		melting	23.32	88.8	
				cooling	22.64	88.5	
	Spent coffee grounds	natural soy wax		melting	45.71	19.43	[40]
				cooling	32.32		
	Delignified balsa	Myristic acid		melting	55.7	179.1	[41]
				cooling	49.6	178.7	
		paraffin		melting	60.3	181.9	
				cooling	56.9	179.4	
	Balsa	n-octadecane	27-35	melting	26.47	49.66	This paper
				cooling	23.75	49.63	
	Cork			melting	27.72	131.2	
				cooling	23.4	131.22	

with balsa was confirmed by the SEM images (Figure 5). The PCM impregnated into the Cork_oct pores accumulated heat during thermal conductivity analysis. The accumulated heat caused heat conduction and fluid (PCM) convection to occur more quickly and strongly. The accumulated heat may also affect the thermal conductivity measurement process. This could be the reason why Cork_oct had a large thermal conductivity value. It

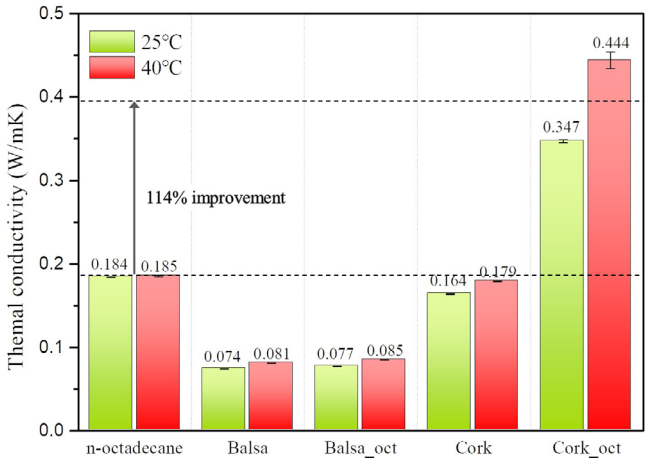

FIGURE 12 Measured thermal conductivity of the PCM, raw materials, and SSPCMs (25°C and 40°C)

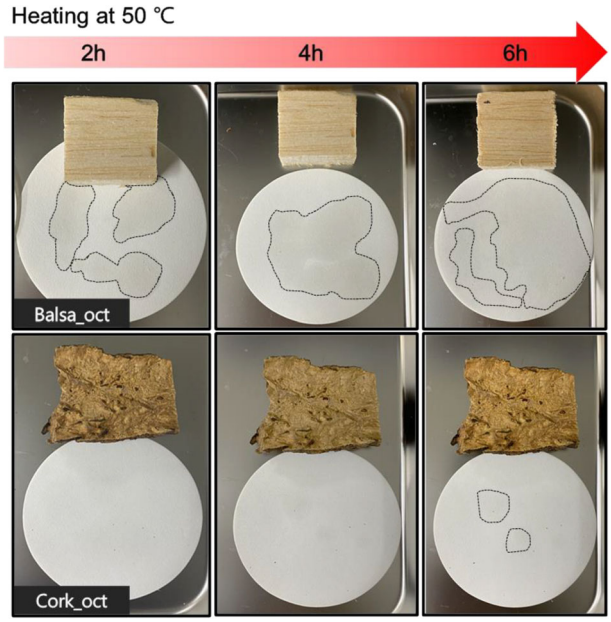

FIGURE 13 Observation of PCM leakage of SSPCM during heating process

can be concluded that the thermal conductivity was affected by the interaction of the PCM with the porous structure of cork. The improved thermal conductivity is an advantage for the heat accumulation by the PCM. Research to improve thermal storage performance by improving the thermal conductivity of PCMs is being actively conducted. Kim et al.[33] fabricated a carbon-based SSPCM by impregnating hexadecane with xGnP. The carbon-based SSPCM showed the improved thermal conductivity, resulting in a 15.7% increase in energy efficiency. By improving the thermal conductivity of pure PCM, balsa- and cork-based SSPCMs are expected to effectively transfer heat to the PCM. The internal porous cell wall enables heat transfer inside the PCM; therefore, it can improve the heat storage capacity of the PCM.

3.5 | Observation of PCM leakage at high temperature of SSPCM

Balsa and cork were used as support materials to stabilize the PCM because of their porous structure and capillary force characteristics. Figure 13 shows the results of the leak test. Figure S2 shows an optical photograph of the prepared specimen, the appearance of which changed at high temperature. Figure 13 shows the change in the filter paper over time, indicating the leakage amount of the SSPCM exposed to high temperatures for 2, 4, and 6 hours. Overall, it can be seen that the PCM leakage behavior occurs actively in Balsa_oct. This is the result of the previous analysis. In particular, the compatibility between PCM and container materials can determine this property. Based on the results analyzed in Chapters 3.1 and 3.2, Balsa is less porous and more hydrophilic than Cork. This makes PCM less compatible and more prone to leaks. It can be inferred that the PCM present in the porous structure at high temperature melts and flows out to the outside as the fixing/supporting power of the PCM container material is insufficient. PCM supporting power is determined by cell structure and chemical compatibility. Cork_oct has a hydrophobic component and at the same time has a very high PCM fixing ability according to the honeycomb structure. The ability is exhibited even at high temperatures, so the amount of PCM leakage is remarkably small. On the other hand, Balsa_oct, PCM leakage occurred gradually after exposure at 50°C for 2 hours. The size of the PCM leakage area also increased over time. A small amount of leakage occurred when Cork_oct was exposed for 6 hours. Balsa_oct, which exhibited severe leakage, had insufficient thermal stability at high temperature. The weight comparison results showed that Balsa_oct and Cork_oct had similar weight gain. However, it can be inferred that the relatively poor thermal performance of Balsa_oct is due to PCM leakage because of its low thermal stability. Cork_oct showed relatively excellent PCM binding ability as a support material, confirming its thermal stability.

4 | CONCLUSION

In this study, balsa and cork were confirmed to have different hierarchical porous structures using SEM images. The chemical composition of cork, specifically suberin, was confirmed by FTIR and EDS mapping.

The improvement in the thermal performance of porous structures using the PCM vacuum-impregnation method was verified. Quantitative, surface/morphological, and chemical analyses were conducted to verify PCM impregnation in the microstructures of balsa and cork. It has been reported that n-octadecane can be integrated into two wood materials. Wood synthetically treated with a PCM (ie, SSPCMs) showed high heat storage capacity, PCM impregnation, and excellent thermal/chemical stability. In particular, Balsa_oct showed an average of heat storage capacity of 49.65 J/g, while Cork_oct showed an average latent heat capacity of 131.21 J/g, which are 20.75% and 54.35% better than the performance of raw PCM, respectively. The thermal conductivity of Cork_oct increased by approximately 114% compared with that of n-octadecane. This allowed rapid heat transfer to the PCM for enhanced heat storage performance. The thermal stability of the SSPCM was evaluated by continuous heating in an oven. In the case of Balsa_oct, PCM leakage occurred during heating for 2 hours at approximately 50°C. In the case of Cork_oct, PCM leakage gradually occurred during 4 hours of heating. However, these were performed at extreme temperatures. The PCM stabilization method will be further developed in the future based on the results of this study. Balsa_oct and Cork_oct have superior heat storage capacity compared with biomaterial-based SSPCMs, and showed average or higher latent heat properties compared with other support materials and PCM composites. Wood has gained increasing attention as a building material because of its sustainability and aesthetically pleasing appearance. This study evaluated its potential as an energy-saving building material by developing the TES capacity of core and bark.

ACKNOWLEDGEMENTS

This work was supported by Korea Institute of Energy Technology Evaluation and Planning (KETEP) grant funded by the Korea government (MOTIE) (20202020800030, Development of Smart Hybrid Envelope Systems for Zero Energy Buildings through Holistic Performance Test and Evaluation Methods and Fields Verifications).

CONFLICT OF INTEREST

The authors declare that they have no known conflicting financial interests or personal relationships that could influence the work reported in this paper.

DATA AVAILABILITY STATEMENT

Author elects to not share data.

ORCID

Jihee Nam https://orcid.org/0000-0003-1365-9616
Ji Yong Choi https://orcid.org/0000-0002-5088-4612
Sumin Kim https://orcid.org/0000-0003-2278-5278

REFERENCES

1. Ummartyotin S, Pechyen C. Strategies for development and implementation of bio-based materials as effective renewable resources of energy: a comprehensive review on adsorbent technology. *Renew Sust Energ Rev*. 2016;62:654-664. doi:10.1016/j.rser.2016.04.066
2. Shirinbakhsh M, Harvey LDD. Net-zero energy buildings: the influence of definition on greenhouse gas emissions. *Energ Buildings*. 2021;247:111118. doi:10.1016/J.ENBUILD.2021.111118
3. Liu B, Gao Q, Liang L, Sun J, Liu C, Xu Y. Ecological relationships of global construction industries in sustainable economic and energy development. *Energy*. 2021;234:121249. doi:10.1016/J.ENERGY.2021.121249
4. Cobut A, Blanchet P, Beauregard R. The environmental footprint of interior wood doors in non-residential buildings - part 1: life cycle assessment. *J Clean Prod*. 2015;109:232-246. doi:10.1016/j.jclepro.2015.04.079
5. Cordier S, Robichaud F, Blanchet P, Amor B. Regional environmental life cycle consequences of material substitutions: the case of increasing wood structures for non-residential buildings. *J Clean Prod*. 2021;328:129671. doi:10.1016/j.jclepro.2021.129671
6. Lehmann S. Low carbon construction systems using prefabricated engineered solid wood panels for urban infill to significantly reduce greenhouse gas emissions. *Sustain Cities Soc*. 2013;6:57-67. doi:10.1016/J.SCS.2012.08.004
7. Himes A, Busby G. Wood buildings as a climate solution. *Dev Built Environ*. 2020;4:100030. doi:10.1016/J.DIBE.2020.100030
8. Osei-Antwi M, De Castro J, Vassilopoulos AP, Keller T. Shear mechanical characterization of balsa wood as core material of composite sandwich panels. *Constr Build Mater*. 2013;41:231-238. doi:10.1016/j.conbuildmat.2012.11.009
9. Borrega M, Gibson LJ. Mechanics of balsa (Ochroma pyramidale) wood. *Mech Mater*. 2015;84:75-90. doi:10.1016/j.mechmat.2015.01.014
10. Wang Q, Lai Z, Luo C, et al. Honeycomb-like activated carbon with microporous nanosheets structure prepared from waste biomass cork for highly efficient dye wastewater treatment. *J Hazard Mater*. 2021;416:125896. doi:10.1016/j.jhazmat.2021.125896
11. De Oliveira H, Yoon B, Michaud V, Do Nam J, Suhr J. All natural cork composites with suberin-based polyester and lignocellulosic residue. *Ind Crop Prod*. 2017;109:843-849. doi:10.1016/j.indcrop.2017.09.044
12. Gallardo-Chacón JJ, Karbowiak T. Sorption of 4-ethylphenol and 4-ethylguaiacol by suberin from cork. *Food Chem*. 2015;181:222-226. doi:10.1016/j.foodchem.2015.02.102
13. Sierra-Pérez J, Boschmonart-Rives J, Dias AC, Gabarrell X. Environmental implications of the use of agglomerated cork as thermal insulation in buildings. *J Clean Prod*. 2016;126:97-107. doi:10.1016/J.JCLEPRO.2016.02.146

14. Silva SP, Sabino MA, Fernandas EM, Correlo VM, Boesel LF, Reis RL. Cork: properties, capabilities and applications. *Int Mater Rev*. 2005;50:345-365. doi:10.1179/174328005X41168
15. Atinafu DG, Yun BY, Yang S, Kang Y, Kim S. Updated results on the integration of metal–organic framework with functional materials toward n-alkane for latent heat retention and reliability. *J Hazard Mater*. 2022;423:127147. doi:10.1016/j.jhazmat.2021.127147
16. Mert MS, Mert HH, Gumus CY. Preparation and characterization of paraffin microcapsules for energy-saving applications. *J Appl Polym Sci*. 2019;136:47874. doi:10.1002/app.47874
17. Chang SJ, Kang Y, Wi S, Jeong SG, Kim S. Hygrothermal performance improvement of the Korean wood frame walls using macro-packed phase change materials (MPPCM). *Appl Therm Eng*. 2017;114:457-465. doi:10.1016/J.APPLTHERMALENG.2016.11.188
18. Saavedra H, García-Herrera C, Vasco DA, Salinas-Lira C. Characterization of mechanical performance of Pinus radiata wood impregnated with octadecane as phase change material. *J Build Eng*. 2021;34:101913. doi:10.1016/j.jobe.2020.101913
19. Li X, Zhu Z, Yang P, et al. Carbonized wood loaded with carbon dots for preparation long-term shape-stabilized composite phase change materials with superior thermal energy conversion capacity. *Renew Energy*. 2021;174:19-30. doi:10.1016/J.RENENE.2021.04.078
20. Li Y, Huang X, Lv J, Wang F, Jiang S, Wang G. Enzymolysis-treated wood-derived hierarchical porous carbon for fluorescence-functionalized phase change materials. *Compos Part B Eng*. 2022;234:109735. doi:10.1016/J.COMPOSITESB.2022.109735
21. Mohammed AM, Elnokaly A, Aly AMM. Empirical investigation to explore potential gains from the amalgamation of phase changing materials (PCMs) and wood shavings, energy. *Built Environ*. 2021;2:315-326. doi:10.1016/J.ENBENV.2020.07.001
22. Chen H, Xuan J, Deng Q, Gao Y. WOOD/PCM composite with enhanced energy storage density and anisotropic thermal conductivity. *Prog Nat Sci Mater Int*. 2022;32:190-195. doi:10.1016/J.PNSC.2022.01.002
23. Nam J, Yang S, Yun BY, Kim S. Evaluation of thermal/morphological performance of SSPCM based nanoclay: influence of the interlayer microstructure of hydrophilic and hydrophobic. *Sol Energy Mater Sol Cells*. 2022;235:111479. doi:10.1016/j.solmat.2021.111479
24. Jeon J, Park JH, Wi S, Yang S, Ok YS, Kim S. Latent heat storage biocomposites of phase change material-biochar as feasible eco-friendly building materials. *Environ Res*. 2019;172:637-648. doi:10.1016/j.envres.2019.01.058
25. Kim YU, Yun BY, Nam J, Choi JY, Wi S, Kim S. Evaluation of thermal properties of phase change material-integrated artificial stone according to biochar loading content. *Constr Build Mater*. 2021;305:124682. doi:10.1016/J.CONBUILDMAT.2021.124682
26. Wi S, Yang S, Lee J, Chang SJ, Kim S. Dynamic heat transfer and thermal performance evaluation of PCM-doped hybrid hollow plaster panels for buildings. *J Hazard Mater*. 2019;374:428-436. doi:10.1016/j.jhazmat.2019.03.136
27. Yilbas BS, Ali H, Al-Sharafi A, Al-Aqeeli N. Droplet dynamics on a hydrophobic surface coated with N-octadecane phase change material. *Colloid Surf A Physicochem Eng Asp*. 2018;546:28-39. doi:10.1016/J.COLSURFA.2018.02.073
28. ASTM E1582-17, Standard Test Method for Temperature Calibration of Thermogravimetric Analyzers'. 2021:1–6. 10.1520/E1582-17.2
29. ASTM C518, Standard Test Method for Steady-State Thermal Transmission Properties by Means of the Heat Flow Meter Apparatus. 2011;06:1–15.
30. ASTM International, ASTM E1461 - 13, Standard Test Method for Thermal Diffusivity by the Flash Method. 2013. 10.1520/E1461-13
31. (ASTM), D7334 - 08, Standard Practice for Surface Wettability of Coatings, Substrates and Pigments by Advancing Contact Angle Measurement, Annu. B. ASTM Stand. 2008;08:1–3. 10.1520/D7334-08R13.2
32. Alkhazaleh AH. Preparation and characterization of isopropyl palmitate/expanded perlite and isopropyl palmitate/nanoclay composites as form-stable thermal energy storage materials for buildings. *J Energy Storage*. 2020;32:101679. doi:10.1016/j.est.2020.101679
33. Kim S, Kim S, Paek S, Jeong SG, Lee JH. Thermal performance enhancement of mortar mixed with octadecane/xGnP SSPCM to save building energy consumption. *Sol Energy Mater Sol Cells*. 2014;122:257-263. doi:10.1016/J.SOLMAT.2013.12.015
34. Lee J, Wi S, Jeong SG, Chang SJ, Kim S. Development of thermal enhanced n-octadecane/porous nano carbon-based materials using 3-step filtered vacuum impregnation method. *Thermochim Acta*. 2017;655:194-201. doi:10.1016/J.TCA.2017.06.013
35. Zhang Z, Alva G, Gu M, Fang G. Experimental investigation on n–octadecane/polystyrene/expanded graphite composites as form–stable thermal energy storage materials. *Energy*. 2018;157:625-632. doi:10.1016/J.ENERGY.2018.06.006
36. Li C, Yu H, Song Y, Wang M, Liu Z. A n-octadecane/hierarchically porous TiO2 form-stable PCM for thermal energy storage. *Renew Energy*. 2020;145:1465-1473. doi:10.1016/J.RENENE.2019.06.070
37. Wi S, Yang S, Park JH, Chang SJ, Kim S. Climatic cycling assessment of red clay/perlite and vermiculite composite PCM for improving thermal inertia in buildings. *Build Environ*. 2020;167:106464. doi:10.1016/J.BUILDENV.2019.106464
38. Ma L, Wang Q, Li L. Delignified wood/capric acid-palmitic acid mixture stable-form phase change material for thermal storage. *Sol Energy Mater Sol Cells*. 2019;194:215-221. doi:10.1016/j.solmat.2019.02.026
39. Sarı A, Hekimoğlu G, Tyagi VV. Low cost and eco-friendly wood fiber-based composite phase change material: development, characterization and lab-scale thermoregulation performance for thermal energy storage. *Energy*. 2020;195:116983. doi:10.1016/J.ENERGY.2020.116983
40. Yoo J, Chang SJ, Wi S, Kim S. Spent coffee grounds as supporting materials to produce bio-composite PCM with natural waxes. *Chemosphere*. 2019;235:626-635. doi:10.1016/J.CHEMOSPHERE.2019.06.195
41. Liu S, Wu H, Du Y, Lu X, Qu J. Shape-stable composite phase change materials encapsulated by bio-based balsa wood for thermal energy storage. *Sol Energy Mater Sol Cells*. 2021;230:111187. doi:10.1016/J.SOLMAT.2021.111187

42. Wang Y, Zhang S, Wang D, Liu Y. Experimental study on the influence of temperature and humidity on the thermal conductivity of building insulation materials. *Energy Built Environ*. 2022. [In press]. doi:10.1016/j.enbenv.2022.02.008

SUPPORTING INFORMATION

Additional supporting information may be found in the online version of the article at the publisher's website.

How to cite this article: Nam J, Yun BY, Choi JY, Kim S. Potential of wood as thermal energy storage materials: Different characteristics depending on the hierarchical structure and components. *Int J Energy Res*. 2022;46(11): 14926-14945. doi:10.1002/er.8195